



**HAL**  
open science

# Experimental Study and Device Design of NO, NO<sub>2</sub>, and NH<sub>3</sub> Gas Detection for a Wide Dynamic and Large Temperature Range Using Pt/AlGa<sub>N</sub>/Ga<sub>N</sub> HEMT

Chris Bishop, Yacine Halfaya, Ali Soltani, Suresh Sundaram, Xin Li, Jérémy Streque, Youssef El Gmili, Paul B Voss, Jean-Paul Salvestrini, Abdallah Ougazzaden

## ► To cite this version:

Chris Bishop, Yacine Halfaya, Ali Soltani, Suresh Sundaram, Xin Li, et al.. Experimental Study and Device Design of NO, NO<sub>2</sub>, and NH<sub>3</sub> Gas Detection for a Wide Dynamic and Large Temperature Range Using Pt/AlGa<sub>N</sub>/Ga<sub>N</sub> HEMT. IEEE Sensors Journal, 2016, 16 (18), pp.6828-6838. 10.1109/JSEN.2016.2593050 . hal-02385234

**HAL Id: hal-02385234**

**<https://hal.science/hal-02385234>**

Submitted on 28 Oct 2022

**HAL** is a multi-disciplinary open access archive for the deposit and dissemination of scientific research documents, whether they are published or not. The documents may come from teaching and research institutions in France or abroad, or from public or private research centers.

L'archive ouverte pluridisciplinaire **HAL**, est destinée au dépôt et à la diffusion de documents scientifiques de niveau recherche, publiés ou non, émanant des établissements d'enseignement et de recherche français ou étrangers, des laboratoires publics ou privés.



Distributed under a Creative Commons Attribution - NonCommercial 4.0 International License

# Experimental Study and Device Design of NO, NO<sub>2</sub>, and NH<sub>3</sub> Gas Detection for a Wide Dynamic and Large Temperature Range Using Pt/AlGaIn/GaN HEMT

Chris Bishop, Yacine Halfaya, Ali Soltani, Suresh Sundaram, Xin Li, Jérémy Streque, Youssef El Gmili, Paul L. Voss, Jean Paul Salvestrini, and Abdallah Ougazzaden

**Abstract**—We report an AlGaIn/GaN HEMT gas sensor designed to enable NO, NO<sub>2</sub>, and NH<sub>3</sub> detection from 100°C–400°C over a large concentration range. Device modeling is performed to optimize several HEMT device parameters for sensing, and the experimental results show that the optimized sensor has improved performance compared with the previously reported HEMT sensors. The device shows significant no sensitivity for the first time in an HEMT device, with sensitivity up to 7% at 400°C. In addition, high sensitivities of up to 17% are reported for NO<sub>2</sub>, and NH<sub>3</sub> is detected at concentrations as low as 150 ppb.

**Keywords**—AlGaIn, GaN, HEMT, sensors, exhaust gas detection

## I. INTRODUCTION

**G**ALLIUM nitride-based chemical sensors have attracted much interest for sensing applications. Gallium nitride devices operate stably at high temperatures and can resist chemical corrosion. GaN-based sensors have even been demonstrated to function in the presence of Cl<sub>2</sub> gas and HCl vapor [1]. Because of these favorable properties, GaN-based sensors are attractive for automotive exhaust applications

where exhaust gas temperatures are elevated. In the context of automobile exhaust, there is strong interest in selectively achieving NO, NO<sub>2</sub>, and NH<sub>3</sub> detection.

While studies using Schottky diode sensors have been reported for NO [2], [3], NO<sub>2</sub> [2], [4]–[7], and NH<sub>3</sub> [8]–[10], there are fewer reports for AlGaIn/GaN high electron mobility transistors (HEMTs). These HEMT sensors are promising for next generation sensing devices because they provide several advantages versus Schottky sensors. First, one may adjust the gate bias to optimize sensitivity. Second, the current to be measured is larger than that of Schottky diodes, yielding higher  $\Delta I = |I_{gas} - I_0|$  and lower theoretical detection limits. Here,  $I_0$  is the initial current under pure N<sub>2</sub> and  $I_{gas}$  is the steady current after the test gas has been applied. Finally, the separation of the current-carrying two-dimensional electron gas (2DEG) from the sensing surface means that at normal operating currents the current flowing through the 2DEG does not interact with the sensing mechanism.

HEMT sensors have reported sensitivity ( $S = \Delta I/I_0$ ) to NO<sub>2</sub> [11] and NH<sub>3</sub> [12], but have not reported significant sensitivity to NO. A Pt/AlGaIn/GaN HEMT structure was shown to exhibit a  $S = 10\%$  to 1000ppm NO<sub>2</sub>, with a high  $\Delta I = 0.5\text{mA}$  at 400°C due to the high initial current of the transistor [11], but no significant response to NO even at concentrations of 3000ppm. A Pt/AlGaIn/GaN HEMT operated in FET mode was shown to have  $\Delta I = 0.64\text{mA}$  and  $S = 2.98\%$  to 35ppm NH<sub>3</sub> at 30°C [12]. The response increased to  $\Delta I = 1.78\text{mA}$  and  $S = 8.25\%$  at 10000ppm, with saturation at concentrations higher than 1000ppm. An AlGaIn/GaN device with 10nm Pt gate was shown to detect NH<sub>3</sub> as low as 35ppm [13] when operated as a Schottky diode. High  $S = 1307\%$  was reported for 150°C, but the  $\Delta I$  was limited to the nA range, illustrating a clear tradeoff between  $S$  and  $\Delta I$ .

In this paper we report an AlGaIn/GaN HEMT sensor using a thin Pt sensing layer that shows improved detection of NO<sub>2</sub>, NO, and NH<sub>3</sub> gases. A model has been implemented to optimize various HEMT parameters for sensing applications, and these simulation results are used to design the improved HEMT sensor. Experimental results are shown and we provide

C. Bishop, P. L. Voss, and A. Ougazzaden are with the School of Electrical and Computer Engineering, Georgia Institute of Technology, Atlanta, GA 30332 USA, and also with Georgia Tech - CNRS, UMI 2958, Metz 57070, France (e-mail: gth837m@mail.gatech.edu; paul.voss@ece.gatech.edu; aougazza@georgiatech-metz.fr).

Y. Halfaya is with the Georgia Tech - CNRS, UMI 2958, Metz 57070, France, and also with PSA Peugeot Citroën, Paris 75116, France (e-mail: yacine.halfaya@mpsa.com).

A. Soltani is with the Institut d'Electronique, de Microélectronique et de Nanotechnologie, UMR-CNRS 8520, COMUE Lille Nord de France, Cite Scientifique, Villeneuve d'Ascq Cedex 59652, France, France (e-mail: ali.soltani@iemn.univ-lille1.fr).

S. Sundaram, X. Li, J. Streque, and Y. El Gmili are with Georgia Tech - CNRS, UMI 2958, Metz 57070, France (e-mail: ssundara@georgiatech-metz.fr; shine.lixin@gmail.com; jstreque@georgiatech-metz.fr; ygmili@georgiatech-metz.fr).

J. P. Salvestrini is with Georgia Tech - CNRS, UMI 2958, 57070 Metz, France, and also with Université de Lorraine, CentraleSupélec, LMOPS, EA4423, Metz 57070, France (e-mail: salvestr@metz.supelec.fr).

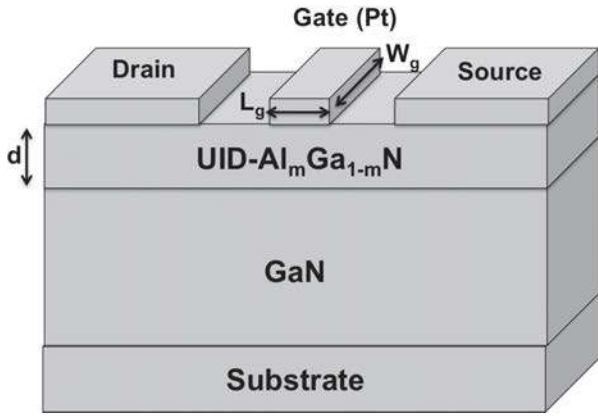


Fig. 1. AlGaIn/GaN HEMT structure used in simulations, with an unintentionally doped (UID) AlGaIn layer.

in-depth characterization of the sensor operation under a large range of concentration of NO, NO<sub>2</sub>, and NH<sub>3</sub> and from 100°C to 400°C. Our results show that HEMT sensors possess stability and sensitivity when detecting NO, NO<sub>2</sub>, and NH<sub>3</sub> gases even at very low concentrations. This is the first time significant sensitivity to NO has been shown using a HEMT-based sensor, and the first time that all three of these exhaust gases have been detected using the same HEMT sensor. It is also the first time that this range of concentrations has been fully studied. We attribute the improved performance of our device to the optimized design. We conclude that it is possible that HEMT sensors may become a key part of diesel anti-pollution systems that are designed to reduce NO and NO<sub>2</sub> pollution, improve fuel efficiency, and meet increasingly stringent regulatory requirements. The paper is organized as follows: Section II summarizes our simulations of the HEMT sensors used for device design. Section III reports AlGaIn/GaN material growth, HEMT device fabrication, and the test setup, and Section IV reports the experimental results and compares them to the literature. Section V concludes.

## II. DEVICE MODELING

### A. Charge Control and I-V Characteristics as a Function of Temperature

The current-voltage characteristics of the AlGaIn/GaN HEMT device shown in Fig. 1 was modeled using the technique by Li and Wang [14]. The current in the channel is represented by

$$I_{ds} = W_g q v(x) n_s(x) \quad (1)$$

where  $W_g$  is the gate width and  $v(x)$  and  $n_s(x)$  are the carrier velocity and sheet carrier density, respectively, at position  $x$  in the channel. The expression for the sheet carrier density is given by the self-consistent solution of the 1-D Poisson's and Schrodinger equations

$$n_s = \frac{\epsilon}{qd} (V_{gs} - V_{th} - E_F) \quad (2)$$

where  $n_s$  is the sheet carrier density in the channel,  $\epsilon = 9.5-0.5m$  is the permittivity of the Al<sub>m</sub>Ga<sub>1-m</sub>N layer [15]

where  $m$  is the aluminum incorporation,  $d$  is the thickness of the AlGaIn layer,  $q$  is the electron charge,  $V_{gs}$  is the applied gate-to-source bias,  $V_{th}$  is the threshold voltage where the device turns off, and  $E_F$  is the Fermi level with respect to the GaN layer conduction band.  $E_F$  is modeled using the equation  $E_F = k_1 + k_2 n_s^{1/2} + k_3 n_s$  where  $k_1$ ,  $k_2$ , and  $k_3$  are calculated for a given temperature using [16]. The nonlinear equations for  $E_F$  and  $n_s$  are solved simultaneously to solve for these parameters.  $V_{th}$  is given by

$$V_{th}(m) = \phi_b(m) - \Delta E_C(m) - \frac{qN_D d^2}{2\epsilon(m)} - \frac{\sigma_{pz}(m)d}{\epsilon(m)} \quad (3)$$

where  $\phi_b$  is the Schottky barrier height,  $\Delta E_C$  is the conduction band discontinuity at the AlGaIn/GaN interface,  $N_D$  is the doping concentration of the AlGaIn layer and  $\sigma_{pz}$  is the polarization sheet charge density at the interface. For  $\sigma_{pz}$ , we use a nonlinear model that includes the spontaneous and piezoelectric polarization as a function of the aluminum incorporation of the AlGaIn layer [17].

The electron drift velocity as a function of the electric field is modeled using a model which accurately describes the drift velocity in both the low-field and velocity-saturation regimes as

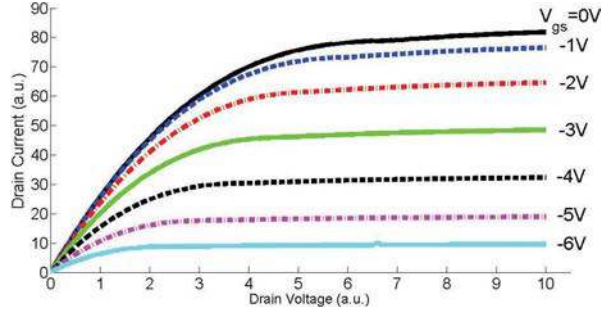
$$v(E) = \frac{\mu_0 E + v_{sat} \left(\frac{E}{E_T}\right)^4}{1 + \left(\frac{E}{E_T}\right)^4 + a \left(\frac{E}{E_T}\right)} \quad (4)$$

where  $v(E)$  is the carrier drift velocity,  $\mu_0$  is the low-field carrier mobility,  $E$  is the electric field in the channel,  $v_{sat}$  is the saturation carrier velocity,  $E_T$  is the critical electric field where  $v(E_T) = v_{sat}$ , and  $a$  models the velocity overshoot effect. We model the low field mobility as a function of the gate voltage using the expression from DasGupta and DasGupta [16]

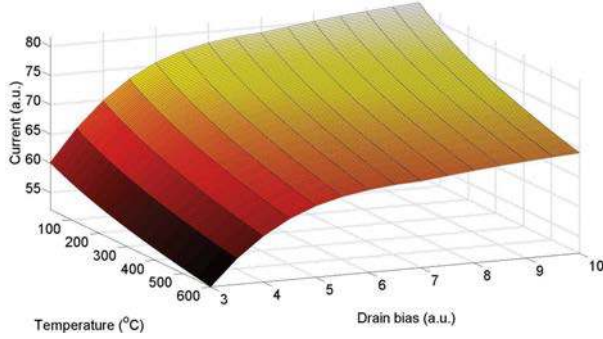
$$\mu_0 = \frac{p_1}{p_2 + (V_{gs} + p_3)^2} \quad (5)$$

where  $p_1$ ,  $p_2$ , and  $p_3$  are experimental coefficients used to determine the mobility as a function of the gate bias.

Expressions for carrier mobility, saturation drift velocity, and energy band offset are implemented to model each of these parameters as a function of temperature [18]. The I-V characteristics are then derived by integrating the channel current along the length of the channel, and defining the voltage and electric field at the drain and source ends for the low-field and velocity-saturation regions as described in [14] in order to obtain two systems of nonlinear equations. Solving these systems of equations gives the drain current for both the low-field and the velocity-saturation regions, which are then combined to give the I-V curve over both regions [14]. The model is implemented in MATLAB using the Trust-Region Dogleg Method to solve the systems of nonlinear equations. The simulated I-V characteristic of the HEMT structure used in this paper is shown as a function of drain and gate bias in Fig. 2(a) and as a function of temperature in Fig.2(b). The simulated I-V curves are consistent with standard device characteristics for AlGaIn/GaN HEMT devices [19].



(a)



(b)

Fig. 2. Model of (a) HEMT I-V curve for various gate voltages and (b) HEMT I-V curve for 25 °C-600 °C.

### B. Gas Sensing Mechanism

Several potential detection mechanisms exist depending on the gas and its behavior with the Pt catalyst and AlGaIn surface [11]. In general, oxidizing and reducing gases such as NO<sub>2</sub> and NH<sub>3</sub> adsorb either on the Pt surface or directly at the AlGaIn surface through pores in the Pt layer. Dissociation reactions on the Pt surface result in gas ions (negatively charged oxygen or positively charged hydrogen for NO<sub>2</sub> and NH<sub>3</sub> gas, respectively) that rapidly diffuse through the gate via pores or grain boundaries and form a chemisorption with adsorption sites at the AlGaIn surface [20], [21]. Another possibility is for the gas molecules or ions that remain on the Pt surface to interact capacitively with the adsorption sites at the AlGaIn surface through the pores [4]. In either case, we model these adsorption sites as electrically charged interface states, most commonly resulting from Ga or N vacancies in the crystal lattice, threading dislocations, or dangling bonds on the surface. To electrostatically balance the charge changes at the interface due to the gas ions, the Schottky barrier height of the gate is changed which can be related to the change in threshold voltage according to equation 3. The dissociation of NH<sub>3</sub> has also been reported to occur only at triple points, where the Pt, gas, and semiconductor surface are all in contact at once [22]. This would require the presence of larger pores for the entire NH<sub>3</sub> molecule to reach the AlGaIn surface. It has also been reported that NO sometimes behaves as a reducing gas, and does not readily dissociate on Pt (therefore also requiring pores for detection). In any case, the voltage shift for dissociative mechanisms, modeled using a Tempkin

isotherm, is expressed as [4]

$$\Delta V = \frac{\rho N_i \theta}{\epsilon \epsilon_0} \quad (6)$$

where  $N_i$  is the concentration of available interface states,  $\rho$  is the dipole moment associated with the chemisorption between the gas ion and interface traps,  $\epsilon$  is the permittivity of the dipole layer.  $\theta$  is the fraction of interface traps bonded by ionized gas molecules and is given by [23]

$$\theta = \frac{K \sqrt{P_{gas}}}{1 + K \sqrt{P_{gas}}} \quad (7)$$

where  $K$  is the equilibrium rate constant that balances the rates of adsorption and desorption, and  $P_{gas}$  is the partial pressure of gas.  $K$  is a function of both temperature and gas concentration, and can be obtained from thermodynamic experiments. This expression for the threshold voltage shift assumes an equilibrium between gas adsorption and desorption, where  $K$  and the surface coverage are not changing with respect to time. For our model, we assume that each of the gas/interface state interactions behaves identically for a particular gas, meaning that we are considering an overall, average effect from these interface states for each gas. Other assumptions include that the probability of dissociation is 1, which is realistic based on experimental observations [4], that all of the reactions occur either on the surface of the Pt gate or at the Pt/AlGaIn interface (i.e. there are no adsorption sites within the continuous Pt layer) and that the ions diffuse readily and rapidly through the thin Pt layer via grain boundaries or pores. Since the purpose of our simulations is to examine general trends in device performance, we do not specify the gas identity and thus our simulations are reported in arbitrary units to reflect this point.

### C. Gate Bias

While the voltage change at the Pt/AlGaIn interface is caused by the interaction of the gate with the gas molecules, it is also possible to apply an additional gate bias to the surface of the gate. This provides a means of tuning the device characteristics in real-time during sensor operation. Simulations of the HEMT sensor sensitivity and absolute current change as a function of the applied gate voltage are shown in Figure 3. It should be noted that while the drain bias may also be used to tune the sensitivity, we have chosen a value in the velocity saturated region in order to ensure device stability and to more easily compare our results with literature. From the simulation results, it is apparent that there is an optimal choice for gate bias in terms of maximizing the current change induced by the presence of the target gas and thus reducing the detection limit. For each gas concentration simulated, the current change approaches zero near the negative threshold voltage, increases as the bias is increased until a maximum value, and then decreases again as the bias becomes more positive. The maximum in  $\Delta I$  is linked to the inflection point of the HEMT transconductance curve. This is the same general trend found in experimental measurements, further supporting the validity of our model [24]. An important observation is that the

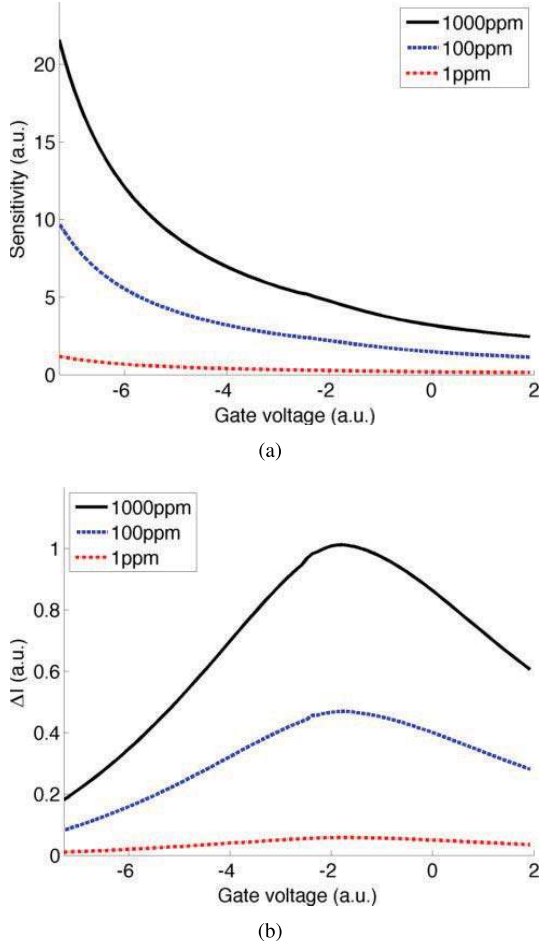


Fig. 3. Simulations of (a) HEMT sensitivity and (b) absolute current change as a function of gate bias ( $V_{ds} = 5V$ ).

device sensitivity follows a different trend, where sensitivity is maximized near the threshold voltage and decreases as the bias is increased. This means that if the device is operated near the threshold voltage, a much higher sensitivity can be achieved at the cost of increasing the detection limit. Therefore, the modulation of gate bias allows for a large adjustable range of sensitivities and detection limits.

Another consideration when applying a bias to the gate is how it will affect the chemical mechanisms regarding the gas adsorption, dissociation, and diffusion on the catalytic sensing area. Localized heating of the gate from an applied bias may also affect the sensing mechanism due to activation of interface traps or favoring certain chemical reactions. Since the  $\Delta I$  is nearly optimal around a 0V gate bias, we choose to use this as an operating point in our first measurements, with the understanding that during real usage the sensitivity can be adjusted by changing the bias. Operation under different gate and drain biases is currently being investigated.

#### D. Gate Dimensions

The gate dimensions and material used in a HEMT sensor are important design considerations because the gate directly interacts with the target gas via a catalytic reaction. In order

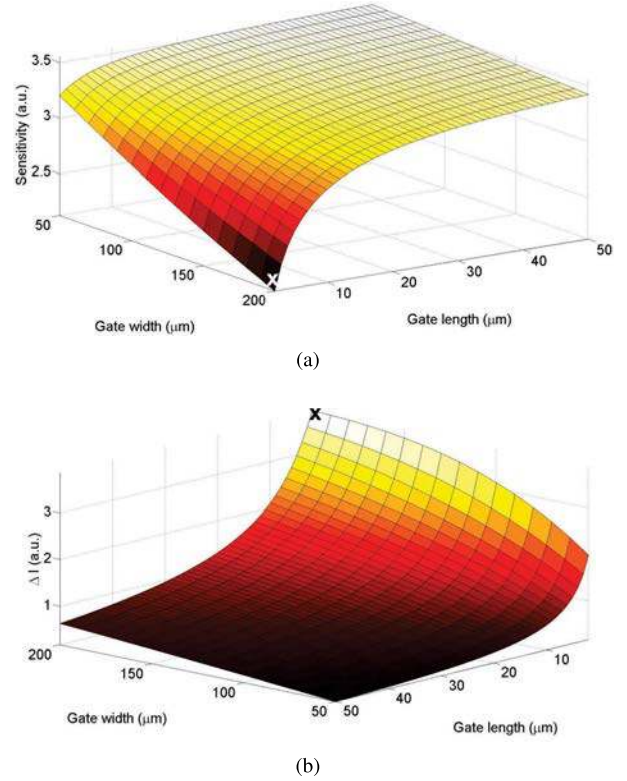


Fig. 4. Simulations of (a) HEMT sensitivity and (b) absolute current change for various gate lengths and widths. x = values for reported device ( $V_{ds} = 5V$ ,  $V_{gs} = 0V$ ).

to evaluate the sensor performance for different gate designs, the sensitivity and  $\Delta I$  of the HEMT sensor was simulated for various gate lengths ( $L_g$ ) and widths ( $W_g$ ) gate bias of 0V. The results are plotted in Figure 4. From these results, we find that the sensitivity is inversely proportional to the aspect ratio ( $W_g/L_g$ ), with a decrease in sensitivity when the gate length is decreased or the gate width is increased. For shorter gate lengths, a higher proportion of the carriers in the 2DEG are above the critical electric field and have saturated velocity, resulting in an increased current over the length of the channel. Since the baseline current is increased, the relative change in current upon gas exposure is decreased, resulting in the observed decrease in sensitivity and increase in  $\Delta I$ . Interestingly, the effect of the gate length on sensitivity seems to be less severe than the effect on  $\Delta I$ ; a small sacrifice in sensitivity lends to a large gain in current and  $\Delta I$ . Another design consideration is the effect of bulk traps and defects on the device current. A longer distance between the source and drain provides a higher probability of an electron interacting with traps and may provide issues with the stability of the device. Therefore we decide to use a smaller gate length ( $2\mu m$ ) so that we retain device stability and have a large  $\Delta I$  with only a small tradeoff in sensitivity.

#### E. Aluminum Incorporation and AlGaN Thickness

Another consideration for fabrication of an AlGaIn/GaN HEMT sensor is the thickness of the AlGaIn layer and the amount of aluminum incorporated in the lattice. The thickness

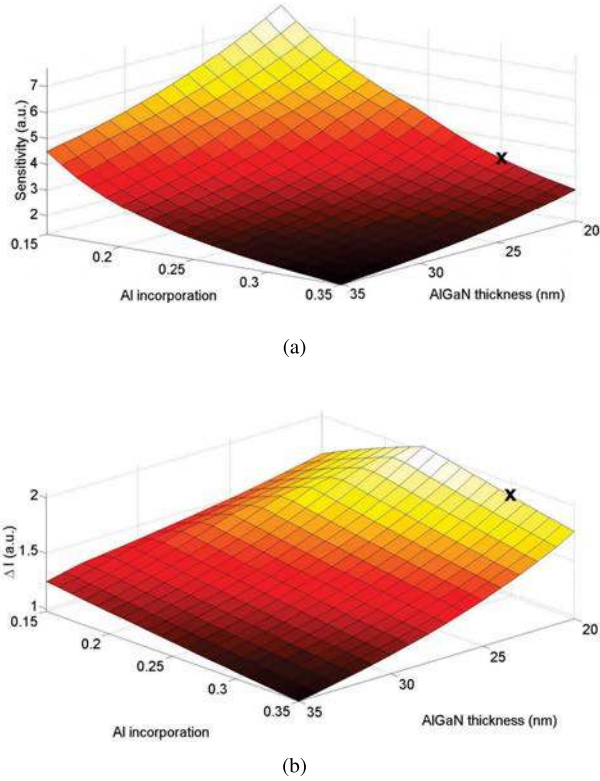


Fig. 5. Simulations of the (a) sensitivity and (b)  $\Delta I$  of the HEMT sensor as a function of AlGaIn thickness and aluminum incorporation.  $x$ -values for reported device ( $V_{ds} = 5V$ ,  $V_{gs} = 0V$ ).

of the AlGaIn layer is directly related to the presence and size of the 2DEG. This is due to the polarization induced at the AlGaIn/GaN interface that results in a net positive charge at this heterointerface and a net negative charge on the surface. Since it is electrostatically favorable to balance this positive charge as close to the charge layer as possible, as the AlGaIn layer thickness increases a negatively charged 2DEG gas forms at the heterointerface and a 2DEG hole gas forms near the surface [15]. Thus, modifying the AlGaIn thickness directly changes the effects of the 2DEG as well as the carriers in channel. In addition, the percentage of aluminum used in the AlGaIn layer of the HEMT sensor determines the threshold voltage due to polarization effects at the AlGaIn/GaN interface from equation 3.

The sensitivity and  $\Delta I$  of the HEMT sensor as a function of the aluminum incorporation and AlGaIn thickness (d) while operating at a fixed 0V gate bias is shown in Figure 5. The simulation is performed for a large range of aluminum incorporations and AlGaIn thicknesses, but it should be noted that not all combinations will result in a 2DEG. Since we have used a simple device model, this factor is not taken into account in the simulation. Thus, care should be taken when designing the HEMT sensor to ensure the parameters result in a 2DEG formation. The results of this simulation follow the same general trend as the gate bias modulation, where the sensitivity of the device is inversely proportional to the aluminum content. The physical explanation for this stems from the fact that a lower aluminum incorporation decreases

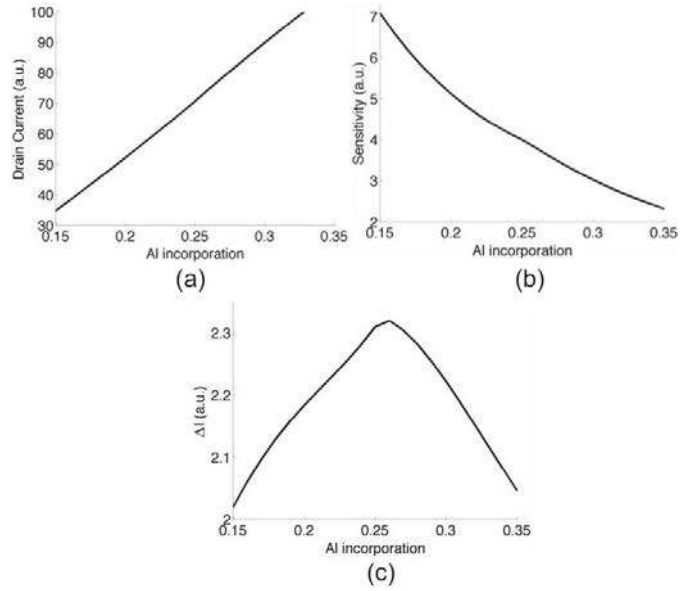


Fig. 6. Simulations of (a)  $I_0$ , (b)  $S$ , and (c)  $\Delta I$  as a function of aluminum incorporation ( $V_{ds} = 5V$ ,  $V_{gs} = 0V$ ).

the initial current of the HEMT, so that the relative change in current is greater when the 2DEG is barely present. However, the device current, and therefore the  $\Delta I$ , measured in this case would be very low, which is seen in our simulation of  $\Delta I$  with varying aluminum incorporation. In terms of the AlGaIn thickness, sensor performance is decreased as the thickness is increased. The explanation stems from the following phenomenon: once the thickness and accompanying electric field are large enough to place carriers in the quantum well, further increases in the AlGaIn thickness do not drastically change the carrier density in the well [25]. Additionally, since the threshold voltage decreases with increased AlGaIn thickness and Al content above the critical values, increasing these parameters while operating at a fixed 0V bias is effectively equivalent to increasing the gate bias. We see that at the optimal AlGaIn thickness of 20nm, the  $\Delta I$  is optimized at aluminum incorporations greater than 25%, and is relatively stable above this value. This is due to the fact that the drain current,  $I_0$ , increases with aluminum incorporation while the sensitivity decreases (see Fig. 6). Therefore,  $\Delta I$ , which is the product of  $I_0$  and  $S$ , reaches an optimal value that balances the two effects. In our design we have chosen an AlGaIn thickness of 20nm and an aluminum incorporation of 30% to have a good balance between  $S$  and  $\Delta I$  while ensuring a 2DEG is formed.

#### F. Pt Thickness

The final design parameter we must consider is the thickness of the Pt gate. It is evident that the morphology and thickness of the gate affects which gas sensing mechanisms are favorable. This phenomenon has been reported for hydrogen and ammonia in Schottky devices [22], and we have previously studied the phenomenon with  $NO_2$ ,  $NO$ , and  $NH_3$  using nitride-based Schottky devices [7]. It has been shown that

TABLE I  
PARAMETERS CHOSEN FOR THE AlGaN/GaN HEMT SENSOR BASED  
ON THE SIMULATIONS USING THE DEVICE MODEL

Parameter	value	units
Gate bias ( $V_g$ )	0	V
Gate length ( $L_g$ )	2	$\mu\text{m}$
Gate width ( $W_g$ )	200	$\mu\text{m}$
Aluminum incorporation (m)	30	%
AlGaN thickness (d)	20	nm
Pt thickness (t)	15	nm

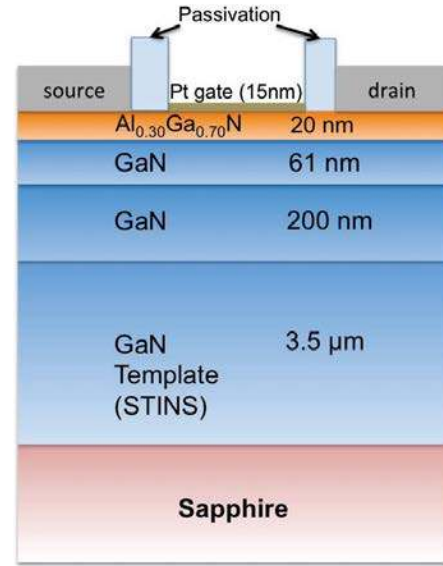
$\text{NH}_3$  can be detected using a 10-20nm Pt gate [12], [13], while sensitivity to NO seems to be lost at thicknesses of at least 75nm [4]. This is most likely due to the fact the NO and  $\text{NH}_3$  require the presence of pores to reach the AlGaN surface, which may not be formed with thicker Pt layers. In our device, we aim to enable sensitivity to each of the three exhaust gases, and therefore we choose to use a thin 15nm Pt gate, with the idea that evaporation of this thickness will form pores in addition to grain boundaries in the Pt layer that will allow the mechanism of each exhaust gas. A summary of the design choices for the AlGaN/GaN HEMT sensor based on our simulations are shown in Table I.

### III. DEVICE FABRICATION/EXPERIMENTAL SETUP

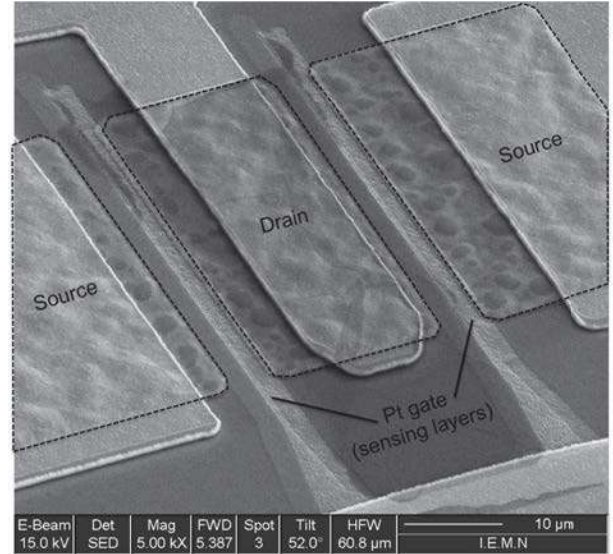
The HEMT structure and processed device are shown in Fig. 7. The devices were grown by MOCVD in a T-shaped reactor [26] using trimethylgallium and ammonia as the gallium, and nitrogen sources, respectively, with nitrogen as the carrier gas. Undoped GaN layers of 200 and 61 nm were grown on an Fe-doped semi-insulating GaN template on a sapphire substrate, followed by 20nm of AlGaN with an Al composition of 30%, which was confirmed by XRD measurements. AFM shows an RMS of 0.77nm and V-defect density of  $1 \times 10^8 \text{cm}^{-2}$ .

For the sensor fabrication, source and drain contacts were defined by optical lithography. The metallization used was based on thermally evaporated Ti/Al/Ni/Au (12/200/40/100 nm) multilayer followed by a rapid thermal annealing at  $870^\circ\text{C}$  for 30s under nitrogen atmosphere. The device isolation is obtained by  $\text{N}_2$  ions multiple implantations. The rectangular-shaped gates were defined by optical lithography with a bi-layer resist stack, and the metallization used was based on electron beam evaporated Pt with a thickness of 15nm, which was measured by profilometry and SEM analysis. The Pt layer shows a high density of pores which is intended to enable and improve detection of all three test gases (see Fig. 8). This step is followed by a  $\text{N}_2\text{O}$  pretreatment for 2 min and a passivation based on  $\text{SiO}_2/\text{Si}_3\text{N}_4$  (100/50 nm) dielectric bi-layer performed by plasma-enhanced chemical vapor deposition at  $340^\circ\text{C}$ . The passivation layer and the active gate area are opened using a  $\text{CHF}_3/\text{CF}_4$  reactive ion etching plasma after be defined by electron beam lithography. Thick interconnection is carried out using evaporated Ti/Au metallization.

For experimental testing, the devices were connected with probes in a gas chamber and connected to a Keithley 236 I-V measurement system. Gas sources of pure  $\text{N}_2$  and varying



(a)



(b)

Fig. 7. (a) AlGaN/GaN HEMT structure. (b) SEM image of processed sensor device

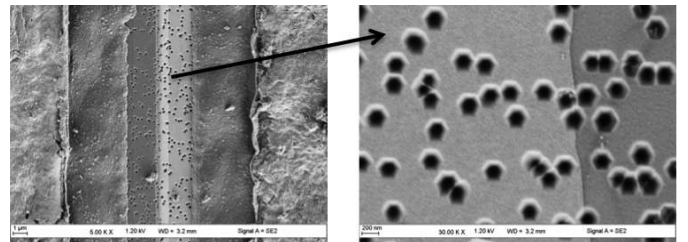


Fig. 8. 15nm Pt gate showing a high density of pores that facilitates gas detection

concentrations of  $\text{NO}_2$ , NO, and  $\text{NH}_3$  with pressure regulators were connected to the testing chamber via a gas blender so that the pressure, concentration, and flow rate were all controlled during the measurements. All experiments were carried out at atmospheric pressure. The temperature was

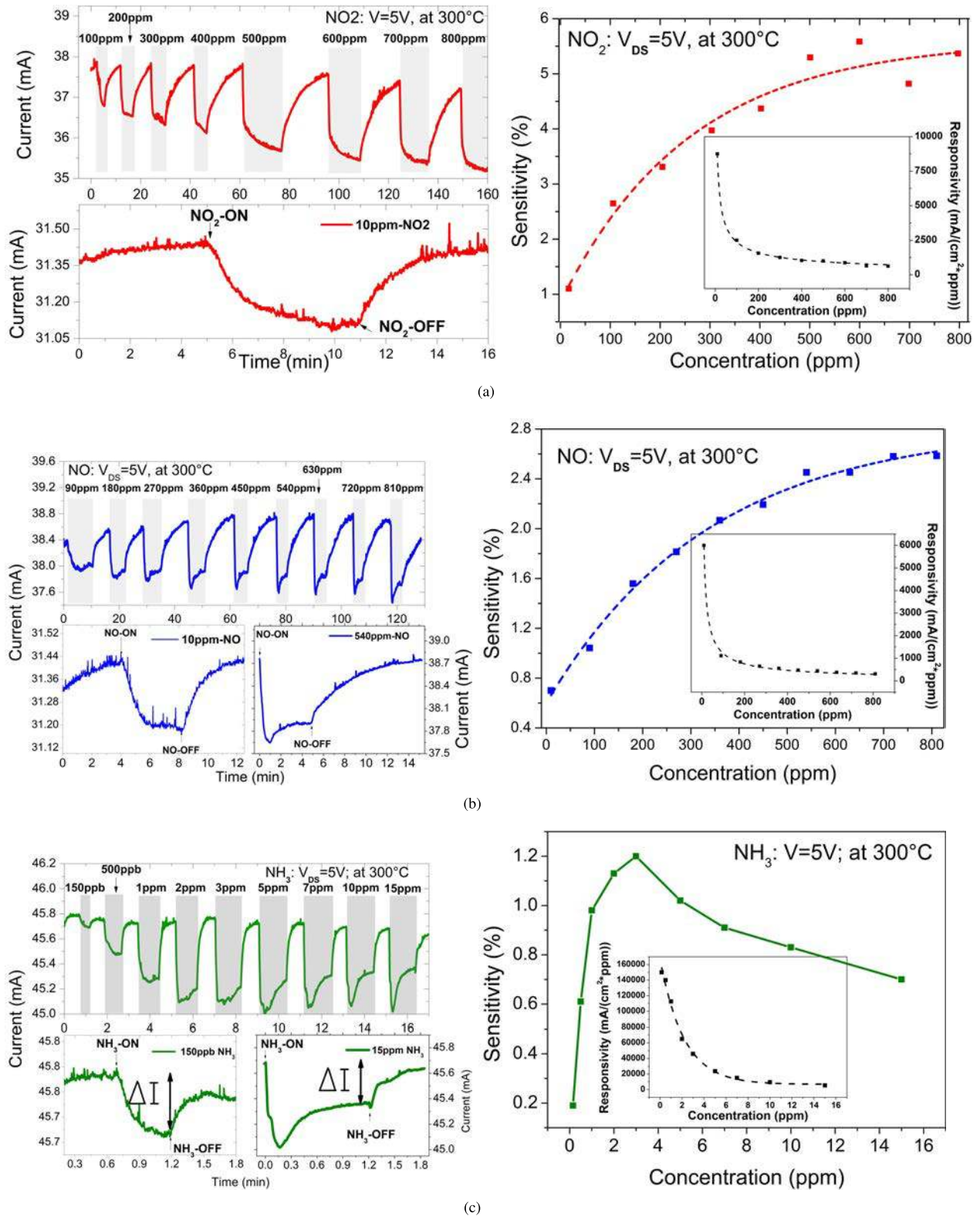


Fig. 9. Experimental results of the AlGaIn/GaN HEMT sensor to (a)  $\text{NO}_2$ , (b)  $\text{NO}$ , and (c)  $\text{NH}_3$  gas, with transient response (left) and sensitivity (right) for various gas concentrations at  $300^\circ\text{C}$ . Responsivity versus concentration is also shown (inset on right).

controlled using an external temperature controller with a heater, and a vacuum pump was used to purge the chamber between gas measurements. A flow rate of 100 sccm was used and with all external factors controlled, we can attribute

any changes in the steady state signal to the gas detection mechanism previously described. For each measurement, the signal under pure  $\text{N}_2$  was used as a reference for comparison with the signal under the test gas in a background of nitrogen.

TABLE II

COMPARISON OF NO<sub>2</sub>, NO, AND NH<sub>3</sub> SENSOR PERFORMANCES, INCLUDING DEVICE STRUCTURE, SENSITIVITY (S),  $\Delta I$ , AND RESPONSIVITY (R)

Gas	Al (%)	d (nm)	$L_g/W_g$ ( $\mu\text{m}$ )	Pt thickness (nm)	$I_0$ (mA)	$\Delta I$ ( $\mu\text{A}$ )	S (%)	R ( $\frac{\text{mA}}{\text{cm}^2 \times \text{ppm}}$ )	C (ppm)	T ( $^\circ\text{C}$ )	Ref.
NO <sub>2</sub>	30	30	70/500	75	5	500	10	1.43	1000	400	[4]
	<b>30</b>	<b>20</b>	<b>2/200</b>	<b>15</b>	<b>16.5</b>	<b>2800</b>	<b>17</b>	<b>1556</b>	<b>450</b>	<b>400</b>	<b>this work</b>
	<b>30</b>	<b>20</b>	<b>2/200</b>	<b>15</b>	<b>35</b>	<b>350</b>	<b>1</b>	<b>8750</b>	<b>10</b>	<b>300</b>	<b>this work</b>
NO	30	30	70/500	75	5	negligible	negligible	negligible	1000	400	[4]
	<b>30</b>	<b>20</b>	<b>2/200</b>	<b>15</b>	<b>11.4</b>	<b>800</b>	<b>7</b>	<b>444</b>	<b>450</b>	<b>400</b>	<b>this work</b>
	<b>30</b>	<b>20</b>	<b>2/200</b>	<b>15</b>	<b>35.7</b>	<b>250</b>	<b>.7</b>	<b>6250</b>	<b>10</b>	<b>300</b>	<b>this work</b>
NH <sub>3</sub>	30	100	N/A	20	5.4e-9	7.6e-8	1307	9.8e-7	35	150	[13]
	38	30	N/A	10	21.5	640	2.98	18286	35	30	[12]
	<b>30</b>	<b>20</b>	<b>2/200</b>	<b>15</b>	<b>45</b>	<b>320</b>	<b>0.7</b>	<b>5333</b>	<b>15</b>	<b>300</b>	<b>this work</b>
	<b>30</b>	<b>20</b>	<b>2/200</b>	<b>15</b>	<b>45</b>	<b>90</b>	<b>0.2</b>	<b>150000</b>	<b>0.15</b>	<b>300</b>	<b>this work</b>

## IV. EXPERIMENTAL RESULTS

The HEMT sensor device was first tested under exposure of various concentrations of NO<sub>2</sub>, NO, and NH<sub>3</sub> at 300°C. For each gas, it was determined that the sensor fully regenerated to its initial current under pure N<sub>2</sub> at a critical temperature between 280-320°C that is dependent on the gas species, while at lower temperatures we were only able to obtain a partial reset. We attribute the reset phenomenon to generating sufficient energy to break the chemical bonds that form between the gas ions and the interface traps at the AlGaIn surface. It should be noted that at temperatures greater than the reset temperature, there remains a static equilibrium between adsorption and desorption under a constant gas flow, and therefore the device is still sensitive to the gas at these temperatures. We analyze the device performance by examining both the transient and steady state responses of the sensor to each gas. For the transient response, the device is exposed to a constant 100sccm flow of the test gas with drain and gate biases of 5V and 0V, respectively, until a steady state value is reached, and then reset under pure N<sub>2</sub>.

The transient response of the HEMT sensor for 10-800ppm NO<sub>2</sub> was measured at 300°C (Fig. 9(a)). This is the first time that this range of concentrations for NO<sub>2</sub> has been studied for HEMT sensors (see Table II). S is shown to increase as a function of concentration. Even at low concentrations of 10ppm,  $\Delta I$  and S were found to be 0.35mA and 1.3%, respectively. At concentrations higher than 600ppm, however, we observe some saturation of both  $\Delta I$  and S, consistent with the results from Schalwig for HEMT devices above 1000ppm. We also see a higher responsivity ( $R = \Delta I / (\text{area} \times \Delta C)$ ), where  $\Delta C$  is the change in gas concentration and the area refers to the gate dimensions  $L_g \times W_g$ ) for lower concentrations, indicating that there is increased performance for concentrations less than 100ppm. The explanation for this may be related to the interface trapping mechanism of the gas species. At low concentrations, a high proportion of the gas molecules are trapped and contribute to the barrier height change. Under higher concentration gas flows, on the other hand, a large number of traps are already filled making it less likely that new gas ions can be trapped at the interface. This observation matches responsivity measurements reported for photodiode devices that is explained by less effective

hole trapping [27], [28]. Since the saturation phenomenon occurs when the interface coverage is maximized, increasing the concentration of interface traps could solve this issue. Another possible explanation may be linked to the available adsorption sites on the Pt catalyst, as well as the available grain boundaries and pores available for gas ion diffusions. It is also important to note that at 300°C the sensor did not fully regenerate to its baseline value in pure N<sub>2</sub>, which is evident by the drift in current over the duration of the measurement. We found that the critical temperature for regeneration after NO<sub>2</sub> exposure is between 310-320°C.

Exposure of the same device to 10-800ppm NO at 300°C showed a  $\Delta I$  and S that also increases as a function of concentration, with saturation beginning after 700ppm (Figure 9(b)). The  $\Delta I$  and S is less than that of NO<sub>2</sub>, with 0.25mA and 0.85%, respectively, for 10ppm NO. This is the first time that this range of concentrations for NO has been studied for HEMT sensors, and the first time that any significant sensitivity has been reported for any concentration of NO using a HEMT device. We note that the ability of our device to sense NO is likely due to the thin Pt layer compared to previously reported HEMT sensors. This is consistent with the fact that some Schottky sensors with Pt thicknesses less than 40nm have also shown some sensitivity to NO [2], [3]. The difference in sensitivity between NO<sub>2</sub> and NO is explained by a difference in detection mechanisms between the two gases. As previously discussed, NO<sub>2</sub> can readily dissociate on the Pt layer into oxygen ions that diffuse through grain boundaries to the AlGaIn surface. NO, on the other hand, does not readily dissociate into oxygen ions; instead, the NO gas molecules must interact directly with traps either at the AlGaIn surface or capacitively through pores in the Pt layer.

Information regarding the chemical reactions between NO and the AlGaIn interface traps can be extracted from the transient response curves. First, we note that the sensor is fully regenerated after NO exposure at only 280°C, which is a lower reset temperature than for NO<sub>2</sub> or NH<sub>3</sub>. This observation supports the idea that the chemical bonds between NO and interface traps at the AlGaIn surface are weaker or that they may be only capacitively linked to the traps from the Pt surface; in either case, less energy is required to break these chemical bonds. We also note that for 10ppm NO, the current under gas flow decreases until steady state, corresponding to a

negative surface potential at the Pt/AlGaIn interface. At higher concentrations, however, we observe an initial decrease followed by an increase in current after a given time. This may be attributed to a second reaction mechanism with a different response time [3], or it may again be related to the number of available interface traps since the behavior depends on the concentration of gas. As the concentration of NO is increased, the increasing portion of the signal, corresponding to a positive surface potential, seems to saturate in magnitude faster than the initial negative peak, and so the overall sensitivity increases. The trend for the responsivity is similar to that of NO<sub>2</sub>, with higher responsivity a lower concentrations. Interestingly, since behavior of the signal response is a function of the concentration, the responsivity may give valuable information about both the types of chemical reactions at the interface as well as the states of the interface traps.

The same experiment was repeated for exposure to NH<sub>3</sub> gas using the same device, with concentrations ranging from 150ppb to 15ppm (Figure 9(c)). Similar to the NO<sub>2</sub> results, a complete reset was not possible for NH<sub>3</sub> at 300°C, but rather in the range of 310-320°C. We report a  $\Delta I$  and S of 0.1mA and 0.2%, respectively, for 150ppb NH<sub>3</sub>. Very high  $R = 150000 \text{ mA}/(\text{cm}^2 \times \text{ppm})$  was found for this concentration, with decreasing responsivity at higher concentrations, as with the other gases. Previously, the lowest reported NH<sub>3</sub> concentration measured using either Schottky or HEMT sensor devices was 35ppm [12], [13]. Interestingly,  $\Delta I$  and S reach a maximum at 3ppm and follow a subsequent decrease as a function of increasing concentration. This is linked to the change in reaction mechanism that begins at 2ppm. At concentrations lower than 2ppm, the signal upon gas exposure decreases until steady state as with NO<sub>2</sub> and low concentrations of NO. At 2ppm, we observe an initial negative peak followed by an increase in signal until steady state is reached, as with higher concentrations of NO. In both cases, we take  $\Delta I$  to be the current change between the initial current and the final steady value, as illustrated in Fig. 9(c). Unlike the NO response, as the concentration is increased, the initial decreasing response saturates while the subsequent increasing response becomes more dominant. It is predicted that at higher concentrations the second reaction mechanism corresponding to a current increase will dominate the total response and the sensor will follow the trends previously reported. The different mechanisms and responses for each gas as a function of concentration provides a viable pathway for completely selective devices, which will be further explored.

To understand how temperature affects the device performance of the HEMT sensor,  $\Delta I$  and S was examined from 100-400°C using an intermediate concentration of 450ppm for NO<sub>2</sub> and NO and 15ppm for NH<sub>3</sub> (Figure 10). For NO<sub>2</sub>, we observe a gradual increase in performance as a function of temperature from 100-300°C followed by a rapid increase up to 400°C. This is attributed to enhanced dissociation of NO<sub>2</sub> and diffusion of oxygen ions at temperatures greater than 300°C. At 400°C, we observe a high sensitivity of 18%, which is much higher than the reported value of 10% for 1000ppm NO<sub>2</sub> at the same temperature. NO exhibits lower  $\Delta I$  and S than NO<sub>2</sub> and reaches peak performance at 300°C, followed

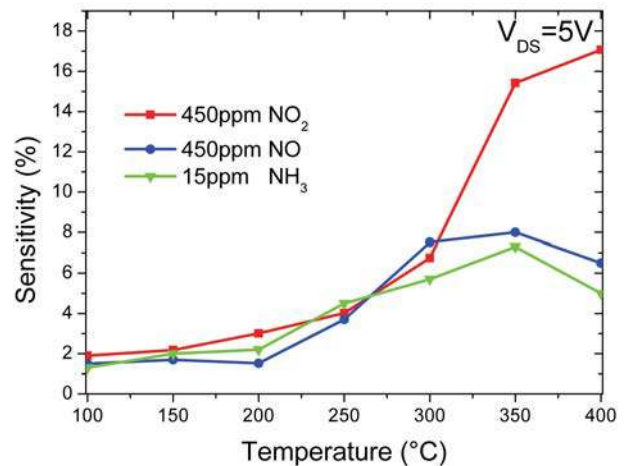


Fig. 10. Sensitivity of 450ppm NO and NO<sub>2</sub> and 15ppm NH<sub>3</sub> from 100 °C-400 °C with 0V gate bias

by a decrease in both metrics. NH<sub>3</sub> behaves similarly, with a peak performance at 350°C. It was found that both the response and recovery times decreased with increasing temperature. Temperature-dependent trap activation may explain the varying behaviors between the three gases, especially between the oxidizing and reducing gases. Self-heating of the HEMT may also play a role in the observed behavior. Heating of the crystal lattice from the applied voltage between the drain and source causes the channel to reach very high temperatures even when the device is operated at room temperature [29]. This may explain why the sensitivity increases significantly for each gas when the temperature is raised above 200°C, since even at lower ambient temperatures the local temperature at the channel may already be near 200°C. The observation of different optimal temperatures may be useful for device selectivity. For example, a commercial device can operate different sensors at different temperatures in order to exclude the response of one or more gases, and to extract specific concentration information from a mixture of exhaust gases. We have performed further analysis of the HEMT sensor operation as a function of temperature in another study [30].

## V. CONCLUSIONS

We have designed, fabricated, and characterized Pt/AlGaIn/GaN HEMT sensors for the improved detection of NO, NO<sub>2</sub>, and NH<sub>3</sub> gases based on optimizations from a model. For NO and NO<sub>2</sub>, we have shown high  $\Delta I$  and S for a range of 10-800ppm. This is the first time that significant response to NO has been realized using a HEMT device, and the first time that this concentration range has been fully studied. The transient and steady state responses show an excellent match to our model and allow us to extract some of the parameters related to the chemical mechanisms. The device also showed high sensitivity to NH<sub>3</sub> over a range of 150ppb-15ppm, which are the lowest concentrations studied using either HEMT or Schottky devices. For NO and NH<sub>3</sub>, we observe different sensor response depending on the gas concentration. We have also shown that the gases behave

differently as a function of temperature, with each gas having a specific optimal temperature. The combination of these sensor properties could be exploited to obtain completely selective devices, which could be used to improve diesel automotive exhaust systems.

## REFERENCES

- [1] K.-A. Son *et al.*, "RF GaN HEMT sensors for detection of caustic chemicals," *IEEE Sensors J.*, vol. 11, no. 12, pp. 3476–3478, Dec. 2011.
- [2] S. A. Khan, E. A. de Vasconcelos, Y. Hasegawa, and T. Katsube, "High-temperature thin-catalytic gate devices for combustion emissions control," *Brazilian J. Phys.*, vol. 34, no. 2b, pp. 577–580, Jun. 2004.
- [3] V. Tilak, K. Matocha, and P. Sandvik, "Pt/GaN Schottky diodes for harsh environment NO sensing applications," *Phys. Status Solidi C*, vol. 2, no. 7, pp. 2555–2558, Jul. 2004.
- [4] J. Schalwig, G. Müller, M. Eickhoff, O. Ambacher, and M. Stutzmann, "Group III-nitride-based gas sensors for combustion monitoring," *Mater. Sci. Eng. B*, vol. 93, nos. 1–3, pp. 207–214, May 2002.
- [5] M. Miyoshi, S. Fujita, and T. Egawa, "Demonstration of NO<sub>x</sub> gas sensing for Pd/ZnO/GaN heterojunction diodes," *J. Vacuum Sci. Technol. B*, vol. 33, no. 1, p. 013001, Jan. 2015.
- [6] V. Van Quang, N. Van Dung, N. S. Trong, N. D. Hoa, N. Van Duy, and N. Van Hieu, "Outstanding gas-sensing performance of graphene/SnO<sub>2</sub> nanowire Schottky junctions," *Appl. Phys. Lett.*, vol. 105, no. 1, p. 013107, Jul. 2014.
- [7] C. Bishop *et al.*, "Highly sensitive detection of NO<sub>2</sub> gas using BGaN/GaN superlattice-based double Schottky junction sensors," *Appl. Phys. Lett.*, vol. 106, no. 24, p. 243504, Jun. 2015.
- [8] I. Lundström, M. Armgarth, A. Spetz, and F. Winqvist, "Gas sensors based on catalytic metal-gate field-effect devices," *Sens. Actuators*, vol. 10, nos. 3–4, pp. 399–421, Nov./Dec. 1986.
- [9] A. Spetz, M. Armgarth, and I. Lundström, "Hydrogen and ammonia response of metal-silicon dioxide-silicon structures with thin platinum gates," *J. Appl. Phys.*, vol. 64, no. 3, pp. 1274–1283, Aug. 1988.
- [10] L. M. Lechuga, A. Calle, D. Golmayo, F. Briones, J. De Abajo, and J. De La Campa, "Ammonia sensitivity of Pt/GaAs Schottky barrier diodes. Improvement of the sensor with an organic layer," *Sens. Actuators B, Chem.*, vol. 8, no. 3, pp. 249–252, Jun. 1992.
- [11] J. Schalwig, G. Müller, M. Eickhoff, O. Ambacher, and M. Stutzmann, "Gas sensitive GaN/AlGaN-heterostructures," *Sens. Actuators B, Chem.*, vol. 87, no. 3, pp. 425–430, Dec. 2002.
- [12] T.-Y. Chen *et al.*, "On an ammonia gas sensor based on a Pt/AlGaN heterostructure field-effect transistor," *IEEE Electron Device Lett.*, vol. 33, no. 4, pp. 612–614, Apr. 2012.
- [13] T.-Y. Chen *et al.*, "Ammonia sensing properties of a Pt/AlGaN/GaN Schottky diode," *IEEE Trans. Electron Devices*, vol. 58, no. 5, pp. 1541–1547, May 2011.
- [14] M. Li and Y. Wang, "2-D analytical model for current–voltage characteristics and transconductance of AlGaN/GaN MODFETs," *IEEE Trans. Electron Devices*, vol. 55, no. 1, pp. 261–267, Jan. 2008.
- [15] O. Ambacher *et al.*, "Two-dimensional electron gases induced by spontaneous and piezoelectric polarization charges in N- and Ga-face AlGaN/GaN heterostructures," *J. Appl. Phys.*, vol. 85, no. 6, pp. 3222–3233, Mar. 1999.
- [16] N. DasGupta and A. DasGupta, "An analytical expression for sheet carrier concentration vs gate voltage for HEMT modelling," *Solid-State Electron.*, vol. 36, no. 2, pp. 201–203, Feb. 1993.
- [17] M. K. Chattopadhyay and S. Tokekar, "Analytical model for the transconductance of microwave Al<sub>m</sub>Ga<sub>1–m</sub>N/GaN HEMTs including nonlinear macroscopic polarization and parasitic MESFET conduction," *Microw. Opt. Technol. Lett.*, vol. 49, no. 2, pp. 382–389, Feb. 2007.
- [18] M. A. Huque, S. A. Eliza, T. Rahman, H. F. Huq, and S. K. Islam, "Temperature dependent analytical model for current–voltage characteristics of AlGaN/GaN power HEMT," *Solid-State Electron.*, vol. 53, no. 3, pp. 341–348, Mar. 2009.
- [19] U. K. Mishra, P. Parikh, and Y.-F. Wu, "AlGaN/GaN HEMTs—An overview of device operation and applications," in *Proc. IEEE*, vol. 90, no. 6, pp. 1022–1031, Jun. 2002.
- [20] I. Lundström, S. Shivaraman, C. Svensson, and L. Lundkvist, "A hydrogen-sensitive MOS field-effect transistor," *Appl. Phys. Lett.*, vol. 26, no. 2, pp. 55–57, 1975.
- [21] I. Lundström and C. Svensson, *Solid State Chemical Sensors*, J. Janata and R. J. Huber, Eds. Orlando, FL, USA: Academic, 1985.
- [22] I. Lundström, "Why bother about gas-sensitive field-effect devices?" *Sens. Actuators A, Phys.*, vol. 56, nos. 1–2, pp. 75–82, Aug. 1996.
- [23] C. Christofides and A. Mandelis, "Solid-state sensors for trace hydrogen gas detection," *J. Appl. Phys.*, vol. 68, no. 6, pp. R1–R30, Sep. 1990.
- [24] H.-T. Wang *et al.*, "Comparison of gate and drain current detection of hydrogen at room temperature with AlGaN/GaN high electron mobility transistors," *Appl. Phys. Lett.*, vol. 87, no. 17, p. 172105, Oct. 2005.
- [25] V. Fiorentini, F. Bernardini, F. D. Sala, A. Di Carlo, and P. Lugli, "Effects of macroscopic polarization in III–V nitride multiple quantum wells," *Phys. Rev. B*, vol. 60, no. 12, pp. 8849–8858, Sep. 1999.
- [26] S. Gautier, C. Sartel, S. Ould-Saad, J. Martin, A. Sirenko, and A. Ougazzaden, "GaN materials growth by MOVPE in a new-design reactor using DMHy and NH<sub>3</sub>," *J. Cryst. Growth*, vol. 298, pp. 428–432, Jan. 2007.
- [27] H. Srour *et al.*, "Solar blind metal-semiconductor-metal ultraviolet photodetectors using quasi-alloy of BGaN/GaN superlattices," *Appl. Phys. Lett.*, vol. 99, no. 22, p. 221101, Nov. 2011.
- [28] J. P. Salvestrini *et al.*, "Tuning of internal gain, dark current and cutoff wavelength of UV photodetectors using quasi-alloy of BGaN-GaN and BGaN-AlN superlattices," in *Proc. SPIE*, vol. 8268, p. 82682S, Jan. 2012.
- [29] B. Benbakhti, A. Soltani, K. Kalna, M. Rousseau, and J.-C. De Jaeger, "Effects of self-heating on performance degradation in AlGaN/GaN-based devices," *IEEE Trans. Electron Devices*, vol. 56, no. 10, pp. 2178–2185, Oct. 2009.
- [30] Y. Halfaya *et al.*, "Investigation of the performance of HEMT-based NO, NO<sub>2</sub> and NH<sub>3</sub> exhaust gas sensors for automotive antipollution systems," *Sensors*, vol. 16, no. 3, p. 273, 2016.